Engineering Analysis with Boundary Elements 92 (2018) 64–72

Contents lists available at ScienceDirect

Engineering Analysis with Boundary Elements

journal homepage: www.elsevier.com/locate/enganabound

A meshfree method with plane waves for elastic wave propagation problems

Svilen S. Valtchev [a,b]

[a] CEMAT–IST, University of Lisbon, Av. Rovisco Pais 1, Lisbon 1049-001, Portugal
[b] Department of Mathematics, ESTG, Polytechnic Institute of Leiria, Portugal

ARTICLE INFO

Keywords:
Elastic wave propagation
Method of fundamental solutions
Asymptotic analysis
Plane waves method

ABSTRACT

In this paper, we address the meshfree numerical solution of time-harmonic linear elastic wave propagation problems in homogeneous media. In particular, we analyze the asymptotic behavior of the method of fundamental solutions (MFS) with source points located far away from the domain of interest. The asymptotic MFS is shown to be equivalent to a Trefftz method, here referred to as the plane waves method (PWM), based on superposition of shear and compressional elastic plane waves with different directions of propagation. Several numerical examples are included in order to illustrate the equivalence between the asymptotic MFS and the PWM. The convergence and stability of the PWM are also analyzed in smooth settings.

1. Introduction

The method of fundamental solutions (MFS) [1–4] is a meshfree and integration free boundary collocation technique that falls into the class of Trefftz methods [5]. In the MFS, the unknown solution of a homogeneous elliptic boundary value problem (BVP) is approximated by superposition of fundamental solutions of the corresponding differential operator, with singularities distributed on a pseudo boundary [6] located in the exterior of the domain.

According to the reported numerical results [7–9], the accuracy of the MFS, when applied in smooth settings, may be improved by increasing the distance between the domain of interest and the pseudo boundary containing the singularities of the shape functions. However, this improvement is limited by the machine precision and the error accumulation due to the ill-conditioning of the corresponding linear systems. In this sense, it is necessary to analyze how far away can we push the singularities in order to achieve accurate numerical results, without destroying the stability of the method.

Besides on the number (and location) of singularities and boundary collocation points, the optimal MFS accuracy depends on the shape of the domain and on the regularity of the boundary conditions, e.g. [9]. In other words, the highest accuracy of the MFS does not necessarily correspond to taking the most distant singularities. The goal of this paper is to analyze the asymptotic behavior of the MFS for far away singularities and not to establish an optimality condition for the MFS accuracy.

The behavior of the classical MFS with source points distributed on a spherical pseudo boundary with an arbitrarily large radius was analyzed in [10,11], for interior acoustic wave propagation problems. In the referred publications it was shown that this asymptotic case of the MFS is equivalent to a meshfree method, called the plane waves method (PWM), based on superposition of acoustic plane waves with different directions of propagation.

Since its introduction, the PWM has been successfully applied for the numerical calculation of eigenfrequencies and eigenmodes of 2D and 3D domains [12] and for estimating eigenmodes for acoustic cavities [13,14]. Also, inverse problems for Helmholtz [15] and Helmholtz-type [16] equations have been solved using the PWM, coupled with the TSVD regularization technique. An efficient matrix decomposition algorithm for solving the PWM linear system was presented in [17], for axisymmetric Helmholtz problems. More recently, a modification of the PWM basis, spanning the same approximation space but reducing significantly the ill-conditioning of the corresponding linear system was proposed in [18].

In this paper we will consider the numerical solution of the Navier equations of elastodynamics via the MFS and analyze its behavior for source points located far away from the domain of interest. In particular, we will show that the solution of the Navier PDE may be represented in terms of the solutions of two Helmholtz equations and consequently, as a linear combination of shear and compressional elastic plane waves. This representation will allow us to extend the PWM to elastic wave propagation problems.

The use of plane waves for the numerical solution of the time-harmonic elastic wave equation is not new. The advantages of such shape functions in comparison with the standard polynomial finite

E-mail address: ssv@math.ist.utl.pt

https://doi.org/10.1016/j.enganabound.2017.10.015
Received 27 July 2017; Received in revised form 15 October 2017; Accepted 16 October 2017
Available online 13 November 2017
0955-7997/

element schemes have been recognized more than two decades ago. Several numerical methods such as the ultra weak variational formulation (UWVF) [19], the discontinuous enrichment method [20] or the variational theory of complex rays [21], among others, have been proposed for simulating elastic wave phenomena. In particular, the use of oscillatory basis functions allows for the accurate solution of medium and high frequency wave propagation problems with lower computational effort, in comparison with the classical FEM. From a theoretical point of view, algebraic order of convergence for linear combinations of elastic plane waves with respect to the dimension of the approximation space and the diameter of the domain has been proven in [22].

The novelty in our work consists in the development and application of a meshfree and integration free method, with elastic plane waves as shape functions, for the numerical solution of the homogeneous Navier equation. The PWM is a Trefftz method and therefore its algorithm is based on the solution of a single collocation linear system for the boundary conditions. Here, the shape functions are operator geared and therefore no numerical or analytical differentiation is also required for the application of the method, as for example if general purpose RBF functions were to be used. In smooth settings, the convergence of the PWM is exponential and thus superior to polynomial finite element methods.

The rest of the paper is organized as follows. In Section 2 we include a brief review of the existing theoretical results for the asymptotic behavior of the classical MFS, when applied to acoustic wave propagation problems. The formulation of the PWM for the numerical solution of the Helmholtz PDE, as introduced in [10], is also recalled. In Section 3 we analyze the asymptotic behavior of the MFS and generalize the PWM from the acoustic (scalar) case to the elastic (vector) case. Section 4 is dedicated to numerical tests illustrating the relation between the asymptotic MFS and the PWM for several elastic wave propagation problems. The convergence and stability of the PWM is also analyzed.

2. Acoustic case

The propagation of a sound wave of small amplitude in a homogeneous isotropic medium $\Omega \subset \mathbb{R}^d$, $d = 2, 3$, with smooth boundary $\Gamma = \partial\Omega$ is modeled by the wave equation. If one is interested in time-harmonic solutions, the problem may be reduced to the solution of a BVP for the Helmholtz equation

$$\begin{cases} \Delta u + k^2 u = 0 & \text{in} \quad \Omega \\ u = g & \text{on} \quad \Gamma \end{cases}, \tag{1}$$

where g is the prescribed Dirichlet boundary condition. If $-k^2$ is not an eigenvalue for the Laplace operator in Ω, or equivalently, if k is not a resonance frequency for the BVP in Ω, problem (1) is well posed and, for C^∞ boundary data, it has a unique solution $u \in C^\infty(\Omega)$, e.g. [23,24].

The fundamental solution for the Helmholtz operator is given by

$$\Phi_k(x) = \begin{cases} \dfrac{i}{4} H_0^{(1)}(k|x|), & d = 2 \\ \dfrac{e^{ik|x|}}{4\pi|x|}, & d = 3 \end{cases} \tag{2}$$

where $H_0^{(1)}$ is the Hänkel function of the first kind and order zero, $|x|$ represents the Euclidian norm in $\mathbb{R}^d$ and i is the imaginary unit. Note that Φ_k exhibits radial symmetry and oscillatory behavior and its real part is singular at $x = 0$.

By shifting the singularity of $\Phi_k(x)$ to an exterior point $y \in \mathbb{R}^d \backslash \bar{\Omega}$, also called a *source point* or *source*, we may define a particular solution for the Helmholtz PDE, given by $\Phi_k(x - y)$, $x \in \Omega$. The classical MFS, e.g. [4,7], consists in approximating the unknown solution of (1) by a linear combination of such fundamental solutions

$$u \approx \tilde{u}(x) = \sum_{j=1}^{n} \alpha_j \Phi_k(x - y_j) \tag{3}$$

where the n source points $y_1, \dots, y_n$ belong to an admissible source point set, also called *artificial boundary* [6], which we will denote by $\hat{\Gamma} \subset \mathbb{R}^d \backslash \bar{\Omega}$. The boundary conditions are then fitted by solving (exactly or approximately) a collocation linear system for a finite set of boundary knots.

2.1. Asymptotic expansions

The following analytic result characterizes the asymptotic behavior of Φ_k for a source point y located far away from the domain of interest Ω, e.g. [25].

Theorem 1. *For $y \in \mathbb{R}^d$ $(d = 2, 3)$ with $|y| \to \infty$ and $x \in \Gamma$ we have*

$$\Phi_k(x - y) = \begin{cases} \dfrac{e^{i\pi/4}}{\sqrt{8k\pi}} \dfrac{e^{ik|y|}}{\sqrt{|y|}} \left(e^{-ikx\cdot\hat{y}} + O\left(\dfrac{1}{|y|}\right)\right), & d = 2, \\ \dfrac{e^{ik|y|}}{4\pi|y|} \left(e^{-ikx\cdot\hat{y}} + O\left(\dfrac{1}{|y|}\right)\right), & d = 3, \end{cases} \tag{4}$$

where[1] *$\hat{y} = y/|y| \in S^{d-1}$ and $(x\cdot y)$ denotes the scalar product in $\mathbb{R}^d$.*

From (4), for $|y| = R >> |\Omega|$ and $x \in \bar{\Omega}$ the fundamental solution $\Phi_k(x - y)$ is asymptotically equivalent to an *acoustic plane wave*

$$\Phi_k(x - y) \sim C_R e^{ikx\cdot\boldsymbol{d}} \tag{5}$$

with the same frequency k, direction of propagation $\boldsymbol{d} = -\hat{y}$ and constant amplitude $C_R = \frac{e^{i\pi/4}}{\sqrt{8\pi k}} \frac{e^{ikR}}{\sqrt{R}}$, for $d = 2$ or $C_R = \frac{e^{ikR}}{4\pi R}$, for $d = 3$. Note that C_R is just a scaling factor for the plane wave.

In view of the above result and noting that acoustic plane waves of the form

$$W_k(x, \boldsymbol{d}) := e^{ikx\cdot\boldsymbol{d}}, \quad \boldsymbol{d} \in S^{d-1} \tag{6}$$

represent particular solutions of the Helmholtz PDE (with frequency k) we may conclude that the MFS with source points located far away from the domain of interest is asymptotically equivalent to a Trefftz method based on superposition of acoustic plane waves with unitary directions of propagation. This meshfree method was formulated and analyzed by Alves and Valtchev in [10] and we refer to it as the Plane Waves Method (PWM).

In the Plane Waves Method, the unknown solution of the BVP is approximated by a linear combination of acoustic plane waves

$$u \approx \tilde{u}(x) = \sum_{j=1}^{n} \alpha_j W_k(x, \boldsymbol{d}_j), \quad x \in \bar{\Omega}, \tag{7}$$

where

$$\mathcal{D} = \{\boldsymbol{d}_j \in S^{d-1} : \ j = 1, \dots, n\} \tag{8}$$

is a prescribed set of n distinct unitary directions. Noting that the plane waves W_k, and therefore $\tilde{u}$, satisfy the Helmholtz PDE, the unknown coefficients $\boldsymbol{\alpha} = (\alpha_1, \dots, \alpha_n) \in \mathbb{C}^n$ are calculated by enforcing the boundary conditions on a set of boundary collocation points. The resulting collocation linear system is usually ill-conditioned and a pseudo-inversion technique (e.g. TSVD) may be requires for its solution, see [26].

The applicability of the PWM may be justified in terms of density results for linear combinations of plane waves in an appropriate functional space defined on Γ, see [10,25]. From a numerical point of view, the performance of the method was analyzed in [10,11] and its equivalence to the asymptotic case of the MFS has been confirmed. Also, exponential convergence of the PWM with respect to the number of collocation points and unitary directions has been observed for BVP posed in smooth domains and with analytic boundary conditions.

[1] Notation: $B_R^d = \{x \in \mathbb{R}^d : |x| < R\}, S_R^{d-1} = \{x \in \mathbb{R}^d : |x| = R\}$, $B^d := B_1^d$ and $S^{d-1} := S_1^{d-1}$.

3. Elastic case

In the absence of body forces, the dynamic equilibrium equations and the constitutive (Hooke's) law for a continuous elastic medium are given by

$$\begin{cases} \sigma_{ij,j} = \rho \ddot{u}_i \\ \sigma_{ij} = \lambda \varepsilon_{kk} \delta_{ij} + 2\mu \varepsilon_{ij} \end{cases}. \tag{9}$$

In (9) the quantities u_i, $\varepsilon_{ij} = \frac{1}{2}(u_{i,j} + u_{j,i})$ and σ_{ij} represent the components of the displacement field $\boldsymbol{u}$, strain tensor $\varepsilon(\boldsymbol{u})$ and stress tensor $\sigma(\boldsymbol{u})$, while $\lambda > 0, \mu > 0$ are the Lamé elastic constants and $\rho > 0$ is the density of the medium. Here we use the Einstein summation convention, δ_{ij} is the Kronecker delta and the indices after the comma denote differentiation with respect to the corresponding variables, e.g. $u_{i,j} = \frac{\partial u_i}{\partial x_j}$.

Combining the two equations from (9) we can derive the equations of motion

$$\mu u_{i,jj} + (\lambda + \mu) u_{j,ji} = \rho \ddot{u}_i, \quad i = 1, \dots, d \tag{10}$$

and assuming time-harmonic variation for the displacement field $\boldsymbol{u}(x,t) = \boldsymbol{u}(x)e^{-i\omega t}$, with ω denoting the circular frequency of vibration, we can obtain an elliptic system of PDEs, also called Navier equations of elastodynamics

$$\mu u_{i,jj} + (\lambda + \mu) u_{j,ji} + \rho \omega^2 u_i = 0, \quad i = 1, \dots, d, \tag{11}$$

which may be rewritten in the following operator form:

$$\mathcal{E}\boldsymbol{u} := \mu \Delta \boldsymbol{u} + (\mu + \lambda) \nabla (\nabla \cdot \boldsymbol{u}) + \rho \omega^2 \boldsymbol{u} = 0. \tag{12}$$

The situation here is more complicated than in the acoustic case, not only because of the vector form of the unknown solution $\boldsymbol{u}$, but also because, for a given frequency ω, there are different types of waves being propagated with different speeds of propagation. The two types of waves that arise are the pressure (dilatation) P-wave and the shear (distortional) S-wave with wave numbers

$$k_p = \omega \sqrt{\frac{\rho}{\lambda + 2\mu}} \quad \text{and} \quad k_s = \omega \sqrt{\frac{\rho}{\mu}}, \tag{13}$$

which depend only on the material properties λ, μ and ρ of Ω.

In the rest of this section we will address the numerical solution of (12) with prescribed displacements on the boundary Γ. More precisely, we will consider the Dirichlet BVP

$$\begin{cases} \mathcal{E}\boldsymbol{u} = 0 & \text{in } \Omega \\ \boldsymbol{u} = \boldsymbol{g} & \text{on } \Gamma \end{cases} \tag{14}$$

posed in a bounded, simply connected domain $\Omega \subset \mathbb{R}^d$ with smooth boundary Γ. In order to simplify the notation we take a normalized density $\rho = 1$.

BVP (14) is well posed, e.g. [27,28], and for a given boundary condition $\boldsymbol{g} \in [C^\infty(\Gamma)]^d$ it has a unique solution $\boldsymbol{u} \in [C^\infty(\Omega)]^d$. As in the acoustic case, the well posedness is guaranteed only if $-\omega^2$ is not an eigenvalue for the (elastostatics) operator $\Delta^* = \mu\Delta + (\lambda + \mu)\nabla\nabla$ in Ω or equivalently if ω is not an eigenfrequency for the BVP (14). We will assume this restriction on the values of ω.

For the elastodynamics operator $\mathcal{E} = -(\Delta^* + \rho\omega^2)$, with $\omega > 0$, the fundamental solution is given by the Kupradze tensor [27]

$$\mathbb{G}_\omega = \frac{1}{\rho\omega^2}\left[k_s^2 \Phi_{k_s} \mathbb{I} + \mathbb{D}\left(\Phi_{k_s} - \Phi_{k_p}\right)\right], \tag{15}$$

where $\mathbb{D} = [\partial^2_{ij}]_{d\times d}$ and Φ_{k_s} and Φ_{k_p} are the fundamental solutions of the corresponding (scalar) Helmholtz equations. Tensor $\mathbb{G}_\omega$ presents radial symmetry, oscillatory behavior and its real part is singular at $x = 0$. For the numerical tests in Section 4 we will consider the simplified form of the Kupradze tensor, as shown in [29].

As in the scalar case, by shifting the singularity of $\mathbb{G}_\omega$ to an exterior point $y \in \mathbb{R}^d \backslash \bar{\Omega}$ we may define a particular solution for the Navier system (14) and the MFS consists in approximating the unknown solution $\boldsymbol{u}$ by a linear combination of the form

$$\boldsymbol{u} \approx \tilde{\boldsymbol{u}}(x) = \sum_{j=1}^{n} \mathbb{G}_\omega(x - y_j) \cdot \mathbf{a}_j, \quad x \in \bar{\Omega}, \tag{16}$$

where the n source points y_j form an admissible source point set $\hat{\Gamma} \subset \mathbb{R}^d \backslash \bar{\Omega}$. The boundary conditions are then fitted by solving (exactly or approximately) a collocation linear system for a finite set of boundary knots. For more details on the application of the MFS to homogeneous and non-homogeneous elastic wave propagation problems we refer the reader to [29,30] and the references therein.

3.1. Asymptotic expansions

Consider the inhomogeneous Navier equations of elastodynamics

$$\mathcal{E}\boldsymbol{u} = \boldsymbol{f} \tag{17}$$

where $\boldsymbol{f}$ is a prescribed body force, with a bounded support. We start with the asymptotic analysis of the solution $\boldsymbol{u}$ in the 2D case. The necessary modifications for the 3D case will be presented afterwards.

2D case: We split the Kupradze tensor $\mathbb{G}_\omega$ into compressional and shear parts

$$\mathbb{G}_\omega = \mathbb{G}_p + \mathbb{G}_s \quad \text{with} \quad \mathbb{G}_p := -\frac{1}{\rho\omega^2}\mathbb{D}\Phi_{k_p} \text{ and } \mathbb{G}_s := \frac{1}{\rho\omega^2}\left(k_s^2 \Phi_{k_s}\mathbb{I} + \mathbb{D}\Phi_{k_s}\right) \tag{18}$$

and consequently separate the solution of (17) into

$$\boldsymbol{u} = -\mathbb{G}_\omega * \boldsymbol{f} = -\mathbb{G}_p * \boldsymbol{f} - \mathbb{G}_s * \boldsymbol{f} := \mathbf{U}_p + \mathbf{U}_s, \tag{19}$$

where $*$ denotes the convolution operator.

For a scalar function G, define the 2D differential operator

$$\nabla^\perp G = \left[G_{,2}, -G_{,1}\right]^\top \tag{20}$$

and note that it satisfies the 2D vector identity

$$\Delta \boldsymbol{u} = \nabla\nabla \cdot \boldsymbol{u} - \nabla^\perp \nabla \times \boldsymbol{u}, \tag{21}$$

where the cross product in 2D is defined as $(u_1, u_2) \times (v_1, v_2) = u_1 v_2 - u_2 v_1$.

Using the properties of the convolution operator and (21) it can be shown that

$$\begin{cases} \mathbf{U}_p = \frac{1}{\rho\omega^2}\nabla\left(\Phi_{k_p} * (\nabla \cdot \boldsymbol{f})\right) \\ \mathbf{U}_s = \frac{1}{\rho\omega^2}\left(\boldsymbol{f} - \nabla^\perp(\Phi_{k_s} * (\nabla \times \boldsymbol{f}))\right). \end{cases} \tag{22}$$

Consequently, the following representation theorem holds for the solution of (17).

Theorem 2. *[2D case] For $x \notin \operatorname{supp} \boldsymbol{f}$, the solution $\boldsymbol{u}$ of (17) can be represented in the following form:*

$$\boldsymbol{u} = \nabla u_p + \nabla^\perp u_s, \tag{23}$$

where $u_p = \frac{1}{\rho\omega^2}\Phi_{k_p} * (\nabla \cdot \boldsymbol{f})$ satisfies the scalar Helmholtz equation

$$\Delta u_p + k_p^2 u_p = f_p \quad \text{with} \quad f_p = -\frac{1}{\rho\omega^2}(\nabla \cdot \boldsymbol{f}) \tag{24}$$

and $u_s = -\frac{1}{\rho\omega^2}\Phi_{k_s} * (\nabla \times \boldsymbol{f})$ satisfies the scalar Helmholtz equation

$$\Delta u_s + k_s^2 u_s = f_s \quad \text{with} \quad f_s = \frac{1}{\rho\omega^2}(\nabla \times \boldsymbol{f}). \tag{25}$$

More precisely, for $x \notin \operatorname{supp} \boldsymbol{f}$, the solution of the BVP (17) may be expressed in terms of the solutions of two scalar Helmholtz equations with frequencies k_p and k_s, respectively.

For the homogeneous case $\boldsymbol{f} = 0$ we have the following corollary of the above result.

Corollary 1. *In the settings of Theorem 2, suppose that* $\boldsymbol{u}$ *satisfies (23), with* u_p *and* u_s *being the solutions of (24) and (25) with* $f_p = 0$ *and* $f_s = 0$, *respectively. Then* $\boldsymbol{u}$ *satisfies the homogeneous Navier equations of elastodynamics* $\mathcal{E}\boldsymbol{u} = 0$.

Proof. Applying (21) we note that

$$\mathcal{E}\boldsymbol{u} = -\mu\nabla^{\perp}\nabla\times\boldsymbol{u} + (\lambda+2\mu)\nabla\nabla\cdot\boldsymbol{u} + \rho\omega^2\boldsymbol{u}. \tag{26}$$

Substituting (23) and using the relations $\nabla\times\nabla = \nabla\cdot\nabla^{\perp} = 0$ and $\nabla\times\nabla^{\perp} = -\Delta$ we derive

$$\mathcal{E}\boldsymbol{u} = \mu\nabla^{\perp}\Delta u_s + (\lambda+2\mu)\nabla\Delta u_p + \rho\omega^2\left(\nabla u_p + \nabla^{\perp}u_s\right). \tag{27}$$

By assumption, u_p and u_s satisfy $\Delta u_p = -k_p^2 u_p$ and $\Delta u_s = -k_s^2 u_s$, respectively. Therefore, using the definitions of k_p and k_s, see (13), we obtain

$$\mathcal{E}\boldsymbol{u} = -\mu k_s^2\nabla^{\perp}u_s - (\lambda+2\mu)k_p^2\nabla u_p + \rho\omega^2\left(\nabla u_p + \nabla^{\perp}u_s\right) = 0, \tag{28}$$

which concludes the proof. □

Applying the acoustic PWM, we may approximate the solutions u_p of (24) with $f_p = 0$ by a linear combination of acoustic plane waves with frequency k_p and unitary directions of propagation $\boldsymbol{d}_j$, $j = 1,\dots,n$, i.e.

$$u_p(x) \approx \sum_{j=1}^{n} \alpha_j e^{ik_p x\cdot\boldsymbol{d}_j}. \tag{29}$$

Analogously, the solution u_s of (25) with $f_s = 0$ may be approximated by

$$u_s(x) \approx \sum_{j=1}^{n} \beta_j e^{ik_s x\cdot\boldsymbol{d}_j}. \tag{30}$$

Next, note that

$$\nabla e^{ik_p x\cdot\boldsymbol{d}_j} = ik_p\boldsymbol{d}_j e^{ik_p x\cdot\boldsymbol{d}_j} \quad\text{and}\quad \nabla^{\perp}e^{ik_s x\cdot\boldsymbol{d}_j} = ik_s\boldsymbol{d}_j^{\perp}e^{ik_s x\cdot\boldsymbol{d}_j} \tag{31}$$

i.e. the application of the operators ∇ and $\nabla^{\perp}$ to an acoustic plane wave results in a P and S elastic plane waves, respectively. Consequently, by (31) and the representation formula (23) we may approximate the solution $\boldsymbol{u}$ of (17) by

$$\boldsymbol{u}(x) \approx \sum_{j=1}^{n} \alpha_j ik_p\boldsymbol{d}_j e^{ik_p x\cdot\boldsymbol{d}_j} + \sum_{j=1}^{n} \beta_j ik_s\boldsymbol{d}_j^{\perp}e^{ik_s x\cdot\boldsymbol{d}_j}, \tag{32}$$

which is essentially, after a redefinition of the coefficients α_j and β_j, a linear combination of elastic P and S plane waves.

3D case: In the 3D case, the vector identity (21) becomes

$$\Delta\boldsymbol{u} = \nabla\nabla\cdot\boldsymbol{u} - \nabla\times\nabla\times\boldsymbol{u}. \tag{33}$$

Also, note that in $\mathbb{R}^3$ the subspace orthogonal to the vector $\boldsymbol{d}$ is two-dimensional and therefore two linearly independent S-waves may be defined.

Theorem 3. *[3D case] For* $x \notin \operatorname{supp}\boldsymbol{f}$, *the solution* $\boldsymbol{u}$ *of (17) can be represented in the following form:*

$$\mathbf{u} = \nabla u_p + \nabla\times\boldsymbol{u}_s, \tag{34}$$

where $u_p = \frac{1}{\rho\omega^2}\Phi_{k_p} * (\nabla\cdot\boldsymbol{f})$ *satisfies the scalar Helmholtz equation*

$$\Delta u_p + k_p^2 u_p = f_p \quad\text{with}\quad f_p = -\frac{1}{\rho\omega^2}(\nabla\cdot\boldsymbol{f}) \tag{35}$$

and $\boldsymbol{u}_s = -\frac{1}{\rho\omega^2}\Phi_{k_s} * (\nabla\times\boldsymbol{f})$ *satisfies the* vector *Helmholtz equation*

$$\Delta\boldsymbol{u}_s + k_s^2\boldsymbol{u}_s = \boldsymbol{f}_s \quad\text{with}\quad \boldsymbol{f}_s = \frac{1}{\rho\omega^2}(\nabla\times\boldsymbol{f}) \tag{36}$$

Proof. Analogous to the 2D case, using (33) instead of (21). □

The representation (34) is also valid in the homogeneous case $\boldsymbol{f} = 0$, with $f_p = 0$ and $\boldsymbol{f}_s = 0$ in (35) and (36). The proof of this result is analogous to the Corollary 1, using (33) and the identities $\nabla\cdot\nabla\times\boldsymbol{u}_s = 0$ and $\nabla\times\nabla u_p = 0$. Also see [22].

As before, the solution u_p of (35) with $f_p = 0$ may be approximated by the acoustic PWM and applying the gradient operator ∇ we obtain the P-wave terms of (32).

On the other hand, the solution of (36) with $\boldsymbol{f}_s = 0$ may be approximated by a linear combination of acoustic plane waves with vector amplitudes $\boldsymbol{q}_j \in \mathbb{R}^3$

$$\boldsymbol{u}_s(x) \approx \sum_{j=1}^{n} \boldsymbol{q}_j e^{ik_s x\cdot\boldsymbol{d}_j}. \tag{37}$$

Noting that

$$\nabla\times\left(\boldsymbol{q}e^{ik_s x\cdot\boldsymbol{d}}\right) = ik_s(\boldsymbol{d}\times\boldsymbol{q})e^{ik_s x\cdot\boldsymbol{d}} \tag{38}$$

we have

$$\nabla\times\boldsymbol{u}_s(x) \approx \sum_{j=1}^{n} ik_s(\boldsymbol{d}_j\times\boldsymbol{q}_j)e^{ik_s x\cdot\boldsymbol{d}_j}, \tag{39}$$

which represents a linear combination of S-waves, since the cross product $(\boldsymbol{d}_j\times\boldsymbol{q}_j)$ is orthogonal to the direction $\boldsymbol{d}_j$. Finally, as in the 2D case, we conclude that the total solution $\boldsymbol{u}$ may be approximated by superposition of P and S elastic plane waves.

3.2. The plane waves method

Summarizing the above results, it is possible to approximate the displacement field $\boldsymbol{u}$ in the Dirichlet BVP (14) by a linear combination of P and S elastic plane waves

$$\begin{cases} \boldsymbol{q}e^{ik_p x\cdot\boldsymbol{d}} & \text{with } \boldsymbol{q}\parallel\boldsymbol{d} \quad \text{(P-wave)} \\ \boldsymbol{q}e^{ik_s x\cdot\boldsymbol{d}} & \text{with } \boldsymbol{q}\perp\boldsymbol{d} \quad \text{(S-wave)} \end{cases} \qquad \boldsymbol{q}\in\mathbb{R}^d,\ \boldsymbol{d}\in S^{d-1}, \tag{40}$$

which, in particular, satisfy the homogeneous Navier system $\mathcal{E}\boldsymbol{u} = 0$. This property allows us to formulate a boundary collocation Trefftz method that generalizes the PWM from the scalar (acoustic) to the vector (elastic) case.

2D case: For a unitary direction $\boldsymbol{d} = (\xi_1,\xi_2) \in S^1$ define the 2×2 tensor

$$\mathbb{W}_{\omega}(x,\boldsymbol{d}) = \begin{bmatrix} \xi_1 e^{ik_p x\cdot\boldsymbol{d}} & \xi_2 e^{ik_s x\cdot\boldsymbol{d}} \\ \xi_2 e^{ik_p x\cdot\boldsymbol{d}} & -\xi_1 e^{ik_s x\cdot\boldsymbol{d}} \end{bmatrix}, \tag{41}$$

where $\mathbb{W}_{\omega}\cdot\mathbf{e}_1$ is a P-wave and $\mathbb{W}_{\omega}\cdot\mathbf{e}_2$ is a S-wave. Here, $\{\mathbf{e}_1,\mathbf{e}_2\}$ denotes the canonical basis of $\mathbb{R}^2$.

Taking a set of distinct unitary directions $\boldsymbol{d}_j \in S^1$, $j = 1,\dots,n$, we may define a plane waves approximation for the displacement field $\boldsymbol{u}$

$$\boldsymbol{u} \approx \tilde{\boldsymbol{u}}(x) = \sum_{j=1}^{n} \mathbb{W}_{\omega}(x,\boldsymbol{d}_j)\cdot\mathbf{a}_j, \tag{42}$$

where the unknown coefficients $\mathbf{a}_j \in \mathbb{C}^2, j = 1,\dots,n$, are calculated so that $\tilde{\boldsymbol{u}}$ satisfies (approximately) the Dirichlet boundary condition on a discrete set

$$\mathcal{X} = \{x_i \in \Gamma :\ i = 1,\dots,m\} \tag{43}$$

of boundary collocation points. Note that (42) is a linear combination of the columns of the tensors $\mathbb{W}_{\omega}(x_j,\boldsymbol{d}_j)$, i.e. a linear combination of P and S waves.

The resulting $(2m)\times(2n)$-dimensional linear system

$$\begin{bmatrix} \mathbb{W}_{\omega}(x_1,\boldsymbol{d}_1) & \cdots & \mathbb{W}_{\omega}(x_1,\boldsymbol{d}_n) \\ \vdots & \ddots & \vdots \\ \mathbb{W}_{\omega}(x_m,\boldsymbol{d}_1) & \cdots & \mathbb{W}_{\omega}(x_m,\boldsymbol{d}_n) \end{bmatrix} \begin{bmatrix} \boldsymbol{a}_1 \\ \vdots \\ \boldsymbol{a}_n \end{bmatrix} = \begin{bmatrix} \boldsymbol{g}(x_1) \\ \vdots \\ \boldsymbol{g}(x_m) \end{bmatrix} \tag{44}$$

is then solved by collocation, if $n = m$ or in the least squares sense, if $m > n$. Regularization techniques, e.g. TSVD, may also be necessary, according to the conditioning of the system.

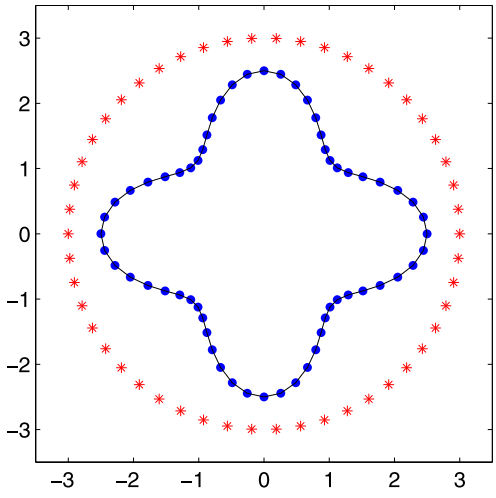

Fig. 1. Sample distribution of collocation and source points for Ω_3.

3D case: For the 3D Dirichlet BVP we should include two linearly independent S-waves in the definition of the plane waves tensor $\mathbb{W}_\omega$. In particular, for a given unitary direction $\boldsymbol{d} = (\xi_1, \xi_2, \xi_3) \in S^2$ we may choose $\boldsymbol{q}_1 = (\xi_2, -\xi_1, 0)$ (note that $\boldsymbol{q}_1 \perp \boldsymbol{d}$) and calculate $\boldsymbol{q}_2 = (\boldsymbol{d} \times \boldsymbol{q}_1) = (\xi_1\xi_3, \xi_2\xi_3, \xi_3^2 - 1)$, but other choices are also possible. For this orthogonal basis of $\mathbb{R}^3$ we define the tensor

$$\mathbb{W}_\omega(x, \boldsymbol{d}) = \left[\boldsymbol{d}e^{ik_p x\cdot\boldsymbol{d}} \quad \hat{\boldsymbol{q}}_1 e^{ik_s x\cdot\boldsymbol{d}} \quad \hat{\boldsymbol{q}}_2 e^{ik_s x\cdot\boldsymbol{d}}\right]_{(3\times 3)}. \tag{45}$$

The PWM is then applied analogously, as in the 2D case. Note that, from a numerical point of view, by taking unitary amplitudes for the plane waves we may improve the conditioning of the PWM collocation matrix. In particular, all columns of the matrix $\mathbb{W}_\omega$ will have the same Euclidian norm.

Remark 1. The method presented here is not restricted to the homogeneous BVP (14). By considering elastic plane waves that vary not only in their direction of propagation but also in their frequency, we may approximate the solution of the inhomogeneous Navier BVP by

$$\boldsymbol{u} \approx \tilde{\boldsymbol{u}}(x) = \sum_{r=1}^{p}\sum_{j=1}^{n} \mathbb{W}_{\omega_r}(x, \boldsymbol{d}_j)\cdot \mathbf{a}_{r,j}, \quad x \in \bar{\Omega}, \tag{46}$$

following the approach presented in [29] for the MFS. Here $\omega_r \in \{\omega_1, \ldots, \omega_p\} \subset \mathbb{R}^+$ is a discrete set of test frequencies and $\boldsymbol{a}_{r,j} \in \mathbb{C}^d$ are unknown coefficients that have to be determined by imposing the PDE and the boundary conditions on appropriate sets of domain and boundary collocation points.

4. Numerical simulations

Three numerical examples, corresponding to three choices for the domain Ω, will be included in this section in order to illustrate the relation between the PWM and the MFS with source points distributed on a circular source set with an arbitrarily large radius R. Additionally, the convergence and stability of the PWM will be analyzed. We will consider only 2D examples but the application of the PWM to BVP posed in 3D domains is analogous, taking into account the corresponding increase in the computational effort.

The PWM will be applied to BVP (14) posed in the following analytic domains:

- a circular domain $\Omega_1 \subset \mathbb{R}^2$ with boundary parameterization:

$$\Gamma_1 = \{(\cos(t), \sin(t)) \in \mathbb{R}^2 \,:\, t \in [0, 2\pi[\} = S^1; \tag{47}$$

- an elliptic domain $\Omega_2 \subset \mathbb{R}^2$ with boundary parameterization:

$$\Gamma_2 = \{(2\cos(t), \sin(t)) \in \mathbb{R}^2 \,:\, t \in [0, 2\pi[\}; \tag{48}$$

Table 1
The maximum absolute error ε_∞ on Γ_1 by the asymptotic MFS and by the PWM. $\omega = 5$.

$n = m$	R^{opt}	MFS	PWM
10	1.585×10^{1}	2.393×10^{-1}	2.673×10^{-1}
15	6.310×10^{2}	4.871×10^{-4}	5.359×10^{-4}
20	6.310×10^{3}	3.122×10^{-7}	3.414×10^{-7}
25	3.981×10^{4}	4.659×10^{-10}	4.514×10^{-10}
30	1.585×10^{3}	7.732×10^{-12}	6.871×10^{-13}

- a star shaped domain $\Omega_3 \subset \mathbb{R}^2$ with boundary parameterization:

$$\Gamma_3 = \{(2 + 0.5\cos(4t))(\cos(t), \sin(t)) \in \mathbb{R}^2 \,:\, t \in [0, 2\pi[\}. \tag{49}$$

Remark 2. Note that if the domain presents singularities, e.g. corners, cracks, cusps, etc., appropriate singular basis functions should be added to the PWM approximation space in order to recreate correctly the singular behavior of the solution in the neighborhood of those points. Such functions have been considered in [31] for the Helmholtz BVP but their extension to the elastic case is out of the scope of this paper.

In the numerical examples, whenever the exact solution of BVP (14) is not available, the quality of the approximate solution will be estimated by measuring its boundary error. This is justified by the well posedness of the BVP, assuming that ω is not an eigenfrequency, and, in particular, by the continuous dependance of the solution on the data given in the problem, e.g. [23].

More precisely, noting that the approximate solution $\tilde{\boldsymbol{u}} = (\tilde{u}_1, \tilde{u}_2)$ satisfies the Navier PDE, there exists a constant $C > 0$ such that the following *a posteriori* error bound holds in smooth settings, e.g. [6]

$$\|\mathbf{u} - \tilde{\mathbf{u}}\|_{\infty,\Omega} \le C\|\mathbf{g} - \tilde{\mathbf{u}}\|_{\infty,\Gamma}. \tag{50}$$

In terms of convergence, this bound guarantees that the numerical method (MFS or PWM) converges, provided the Dirichlet boundary condition can be approximated with an arbitrarily high accuracy. The latter is guaranteed by the available density results for fundamental solutions [29] and plane elastic waves [22] in appropriate functional spaces defined on Γ, e.g. in $[L^2(\Gamma)]^2$ or $[C^\infty(\Gamma)]^2$.

From a numerical point of view, the boundary error $\|\mathbf{g} - \tilde{\mathbf{u}}\|_{\infty,\Gamma}$ will be estimated by measuring the maximum absolute error

$$\varepsilon_\infty := \max_{1\le j\le 2}\max_{z\in\mathcal{Z}} |u_j(z) - \tilde{u}_j(z)|, \tag{51}$$

for a discrete set $\mathcal{Z} \subset \Gamma$ of $3\times m$ error test points.

An example of collocation and source point distributions is shown on Fig. 1. The boundary knots will be distributed uniformly, with respect to the parameter t in the boundary parametrization.

Example 1. Consider the Dirichlet BVP for the Navier equations of elastodynamics, posed in Ω_1. For the boundary condition on Γ_1 we took the smooth function

$$\boldsymbol{g}_1(x) = \big(\sin(x_1 + ix_2)\ ;\ i\cos(x_2)\big), \qquad x \in \Gamma_1 \tag{52}$$

and fixed $\lambda = \mu = \rho = 1$ and $\omega = 5$. Note that, for this example, the exact solution of BVP (14) is not available and we will use the value of the boundary error ε_∞ as an indicator for the accuracy of the approximate solution.

The variation of the numerical precision of the MFS, as a function of R, is illustrated in Fig. 2. For small values of R, see left plot, the accuracy of the method increases until $R \approx 3$ and is approximately constant for $3 \le R \le 10$. Further increase in the distance between the source points and the collocation points may lead to a significant improvement of the results. For example, in the case $n = m = 30$, the optimal precision of the MFS is achieved at $R^{opt} \approx 10^3$, see right plot. The corresponding value of the absolute error, $\varepsilon_\infty^{opt} = 7.8151\times10^{-12}$, may be viewed as the precision of the asymptotic MFS. For larger values of R the numerical results begin to deteriorate due to rounding error accumulation and insufficient machine precision.

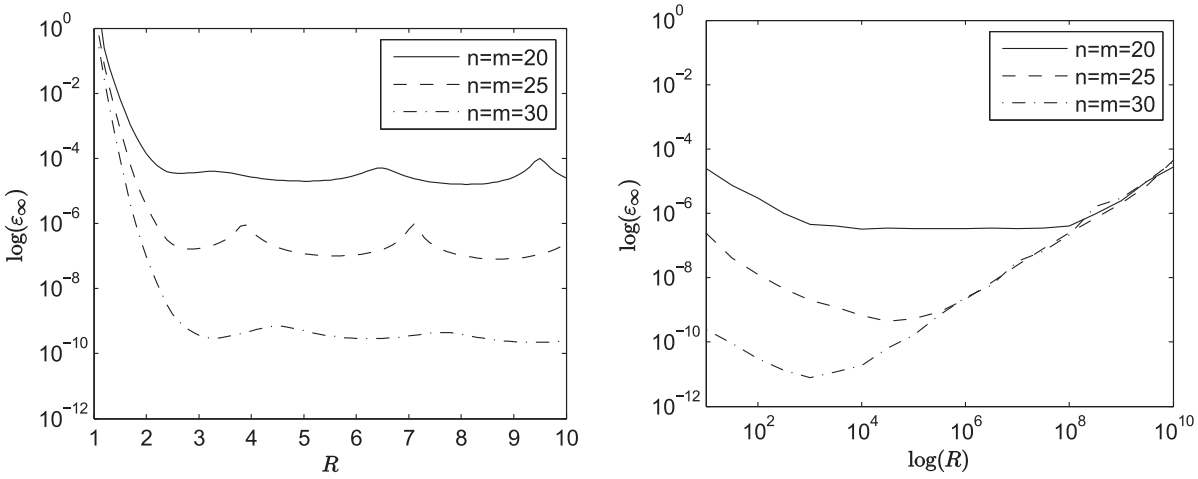

Fig. 2. The precision of the MFS as a function of $R \in [1.1, 10]$ (left) and $R \in [10, 10^{10}]$ (right).

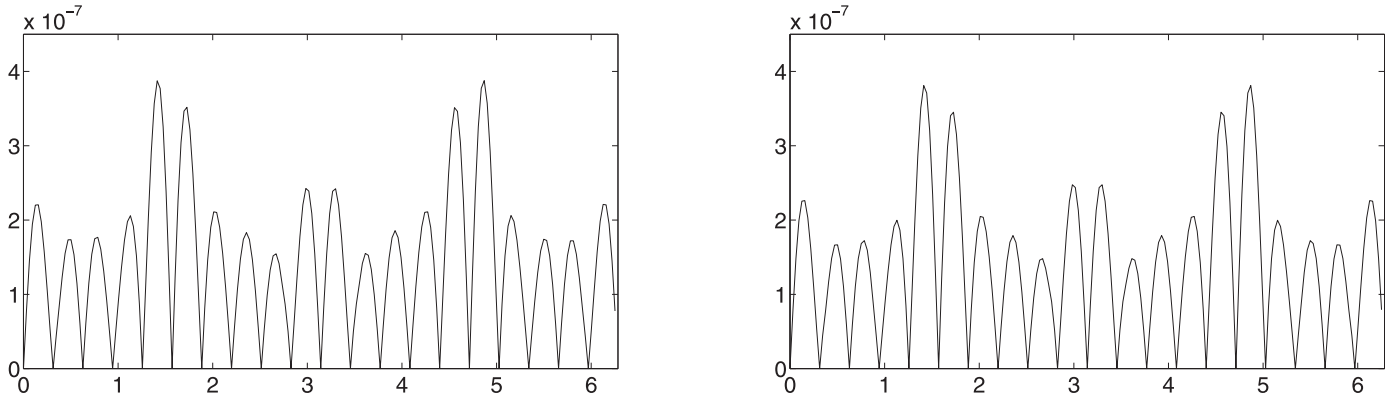

Fig. 3. The absolute error on Γ_1 by the MFS (left, $R = 5 \times 10^4$) and by the PWM (right).

Table 2
The maximum absolute error ε_∞ on Γ_1 by the MFS with $R = 10^4$ and by the PWM.

ω	$n = m$	MFS	PWM
10	30	2.024×10^{-8}	2.024×10^{-8}
15	36	6.873×10^{-8}	6.872×10^{-8}
20	43	1.983×10^{-8}	1.982×10^{-8}
25	50	2.427×10^{-8}	2.428×10^{-8}
30	55	3.208×10^{-8}	3.204×10^{-8}

In Table 1 we present numerical results by the asymptotic MFS and by the PWM for several knot configurations. These results confirm that the PWM is at least as accurate as the asymptotic MFS. Here the value of R^{opt} was determined by analyzing the accuracy of the MFS for $R \in [1.1, 10^{10}]$. For $R < R^{opt}$ or $R > R^{opt}$ the MFS is less accurate than the PWM.

The boundary error profiles for the PWM and for the asymptotic MFS are also similar. In Fig. 3 we present the plots of the absolute error on Γ_1 by the two methods. For this simulation we considered $n = m = 20$ and took $R = 5 \times 10^4$ for the MFS.

We also compared the PWM and the MFS for higher values of the frequency ω. The equivalence of the two methods is illustrated in Table 2. Here we selected the values of the parameters $n = m$ in the MFS such that an absolute error $\varepsilon_\infty \sim 10^{-8}$ could be achieved. Also, for the MFS we considered $R = 10^4$ which corresponds to the asymptotic precision of the method. In this simulation the MFS started losing precision for $R > 10^6$, due to the rounding error accumulation.

We conclude this example with a convergence and stability analysis of the PWM with respect to the number of collocation points and unitary directions. Due to the smoothness of this example we will consider $n = m$.Fig. 4(left) illustrates the evolution of the maximum absolute error in a semi-log scale. The graphical results indicate that the absolute error starts decreasing as soon as $n = m = \omega$, i.e. when one knot per unit frequency is considered. However, accurate numerical results require at least 1.5 knots per unit frequency. For example, in the case $\omega = 40$ the convergence of the PWM starts when $n = m = 40$ but errors lower than 10^{-5} are observed only for $n > 60$ knots. In the region of convergence, the graphical results suggest an exponential rate of convergence for the PWM, similar to the one observed for the classical MFS.

On the other hand, when the machine precision is reached, i.e. for $\varepsilon_\infty \leq 10^{-14}$, no further improvement of the numerical results is possible by increasing the number of collocation points and unitary directions. An interesting fact is that, even after exhausting the machine precision, the PWM remains relatively stable. This fact is related with the conditioning of the PWM linear system (44), see Fig. 4(right). Similar to most meshless methods based on global approximation of the solution, the condition number of the corresponding matrix increases exponentially with respect to its dimension. However, comparing the two plots in Fig. 4, we noticed that when the ε_∞ reaches its minimum value of 10^{-15} the condition number of the matrix is still approximately 10^5, which allows for the accurate solution of the linear system. PWM becomes unstable only after the condition number of the matrix reaches values of order 10^{17}.

Example 2. We considered the elliptic domain Ω_2 and a Dirichlet boundary condition

$$g_2(x) = \big(\sin(x_1 x_2)\exp(i x_1)\ ;\ i\cos(x_2)\big), \qquad x \in \Gamma_2. \tag{53}$$

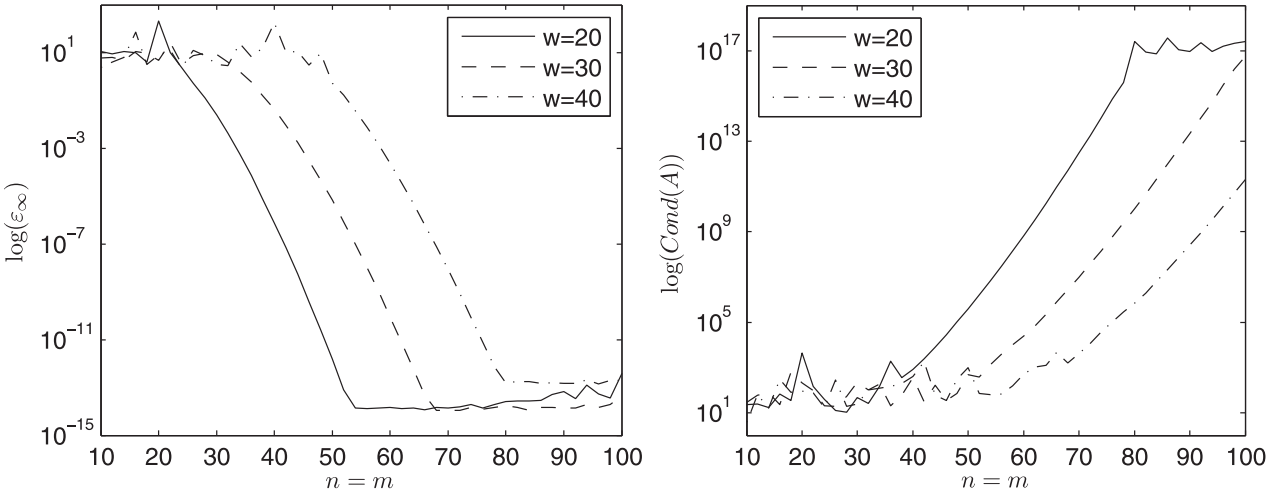

Fig. 4. The maximum absolute error ε_∞ by the PWM (left) and the condition number $Cond(A)$ of the corresponding linear system (right), as functions of $n = m$. Semi-log scale.

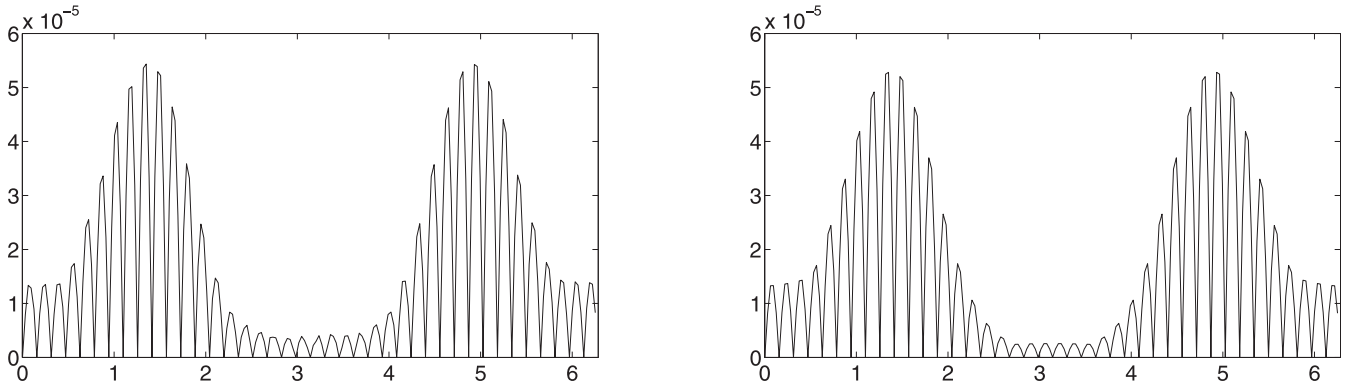

Fig. 5. The absolute error on Γ_2 by the MFS (left) and by the PWM (right). $\omega = 10$.

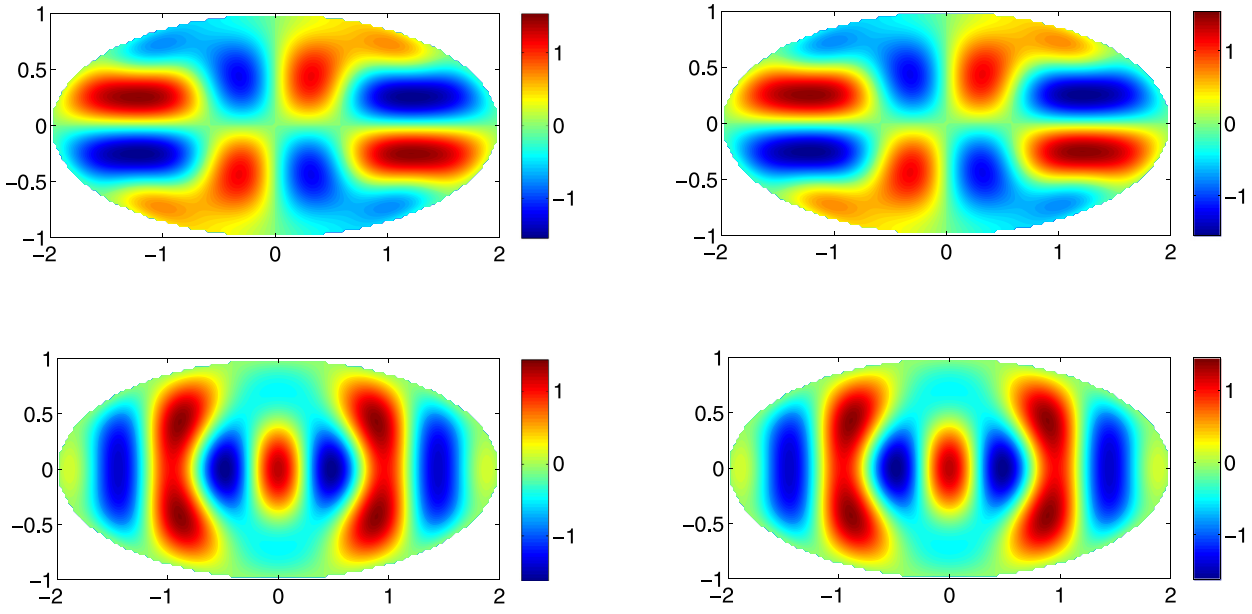

Fig. 6. The real part of the components of $\tilde{\boldsymbol{u}}$. MFS (left column) and PWM (right column). $\omega = 10$.

For the Lamé constants we took $\lambda = 3$ and $\mu = 2$ and for the density $\rho = 1$. As in the previous example, the exact solution of BVP (14) with boundary condition $\boldsymbol{g}_2$ is not known and the accuracy of the approximate solution will be analyzed by measuring its boundary error ε_∞.

The graphical results for the boundary error by the two methods with $\omega = 10$, $n = m = 40$ and $R = 8 \times 10^5$ are shown in Fig. 5. The global behavior of the absolute error and its magnitude are similar for the two methods. Taking $5 \times m$ boundary points, we measured $\varepsilon_\infty = 5.436 \times 10^{-5}$ for the MFS and $\varepsilon_\infty = 5.282 \times 10^{-5}$ for the PWM.

In the interior of the domain the approximate solutions by the two methods are also undistinguishable, see Fig. 6.

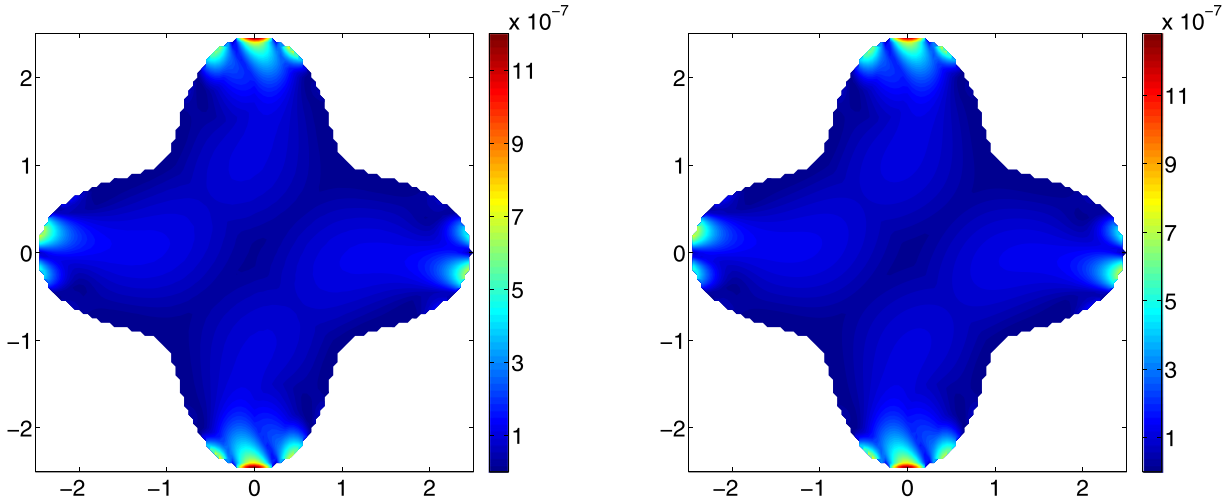

Fig. 7. The absolute error in Ω_3, by the MFS (left) and by the PWM (right).

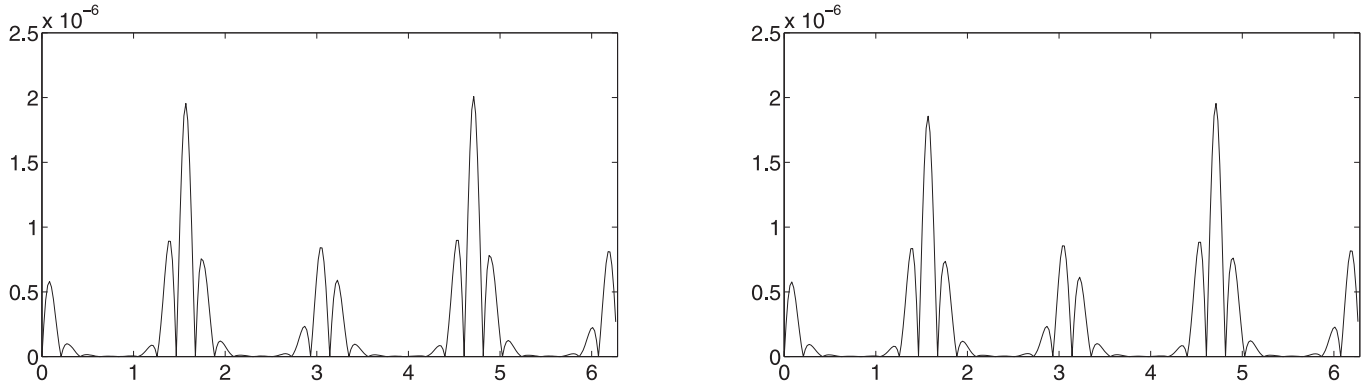

Fig. 8. The absolute error on Γ_3, by the MFS (left) and by the PWM (right).

Table 3
The maximum absolute error ε_∞ on Γ_2 and the condition number of the linear system for the MFS (with $R = 10^4$) and for the PWM. $\omega = 2$.

$m\ (=2n)$	MFS *Cond*(*A*)	MFS ε_∞	PWM *Cond*(*A*)	PWM ε_∞
20	8.979×10^{2}	8.091×10^{-2}	4.267×10^{2}	8.097×10^{-2}
30	3.230×10^{5}	1.575×10^{-2}	1.439×10^{5}	1.498×10^{-2}
40	2.838×10^{8}	1.082×10^{-3}	1.592×10^{8}	1.077×10^{-3}
50	4.141×10^{11}	6.487×10^{-5}	3.214×10^{11}	6.042×10^{-5}

Table 4
The maximum absolute error ε_∞ on Γ_3 by the MFS with $R = 10^6$ and by the PWM.

ω	$m\ (=2n)$	MFS	PWM
10	100	1.186×10^{-4}	1.188×10^{-4}
15	150	3.298×10^{-6}	4.297×10^{-6}
20	200	6.408×10^{-7}	1.219×10^{-7}
25	250	9.778×10^{-9}	1.299×10^{-8}
30	300	6.377×10^{-9}	3.834×10^{-10}

In Table 3 we include the numerical results from the two methods, for a lower frequency $\omega = 2$. Also, we considered twice as many collocation points as directions/sources ($m = 2n$) for this simulation and solved linear system (44) in the least squares sense. For the MFS we took $R = 10^4$.

The numerical results in Table 3 indicate that the PWM is slightly more accurate than the asymptotic MFS due to the slightly better conditioning of the PWM linear system. However, in terms of order of magnitude, the two methods show similar precision and stability.

Example 3. Consider the Dirichlet BVP for the star-shaped domain Ω_3 and the boundary condition

$$g_3(x) = \mathbb{G}_\omega(x-y)(\mathbf{e}_1+\mathbf{e}_2) + \mathbb{W}_\omega(x,\boldsymbol{d})(\mathbf{e}_1+\mathbf{e}_2), \qquad x\in\Gamma_3, \tag{54}$$

where $y = (5,-5) \notin \tilde{\Omega}_3$ and $\boldsymbol{d} = (1,1)/\sqrt{2}$. We fixed $\lambda = \rho = 1$ and $\mu = 2$. Note that the natural extension (from Γ_3 to Ω_3) of function $\boldsymbol{g}_3$ is also the exact solution of BVP (14) and, for this example, it is possible to measure the absolute error of $\tilde{\mathbf{u}}$ in $\tilde{\Omega}_3$ explicitly.

The absolute error of the approximate solution in Ω_3, by the two methods, is shown in Fig. 7. Here we considered $\omega = 3$, $n = m = 30$ and $R = 10^5$ for the MFS.

The two plots are similar, with the absolute error assuming its peak values near the points of the star shaped domain. On the boundary of the domain the numerical results are also approximately the same, see Fig. 8. On Γ_3 we measured $\varepsilon_\infty = 2.008\times10^{-6}$ by the MFS and $\varepsilon_\infty = 1.955\times10^{-6}$ by the PWM.

Accurate numerical results were also obtained for higher values of the circular frequency ω, see Table 4. Here we considered 10 collocation points per unit frequency, i.e. $m = 10\times\omega$, due to the complexity of the domain Ω_3. Also, we took $R = 10^6$ for the asymptotic MFS and a knot configuration with $m = 2n$, which improved the condition number of the collocation matrices by approximately 3 orders of magnitude, in comparison with the case $m = n$. The boundary errors were measured on $5\times m$ knots.

During the numerical simulations we noticed that the MFS was significantly slower than the PWM. In order to illustrate this fact we measured the CPU time necessary to build the collocation matrix in the two methods, see Table 5. We took $\omega = 3$ and $R = 10^4$ for the asymptotic MFS. The two methods were coded in Matlab and a laptop with an Intel Core i7 640M CPU running at 2.8 GHz was used.

Table 5
The CPU time (in seconds) required to build the collocation matrix for the MFS and the PWM.

$n = m$	MFS	PWM
10	0.040	0.016
20	0.127	0.023
40	0.422	0.055
80	1.637	0.185
160	6.504	0.760

By analyzing the numerical results in Table 5, we may conclude that the difference in the speed of the two methods increases with the increase in the dimension of the matrix. For example the MFS is 2.5 times slower than the PWM for $n = m = 10$ but this difference increase to approximately 9 times for $n = m = 25$. This advantage of the PWM is due to faster routines for evaluating exponential functions (plane waves) in comparison with the routines for evaluating the Hänkel function (fundamental solutions). Note that for large scale problems the most time consuming part of the methods becomes the actual solution of the linear system and the two methods will have approximately the same run time.

5. Conclusions

An asymptotic analysis of the method of fundamental solutions with source points located far away from the domain of interest has been performed for 2D and 3D elastic wave propagation problems in homogeneous media. In particular, it has been shown that the asymptotic MFS is equivalent to a meshfree boundary collocation method, based on superposition of shear and compressional elastic plane waves. The method described here can be viewed as an extension, from the scalar (acoustic) case to the vector (elastic) case, of the plane waves method (PWM) analyzed in [10].

The equivalence between the asymptotic MFS and the PWM has been illustrated through several numerical examples, for different geometries and boundary conditions. Also, this equivalence holds even for BVPs with high circular frequencies. The numerical results indicate that, in smooth settings, the PWM is an accurate and robust meshfree numerical method which converges exponentially for the solution of the Navier equations of elastodynamics.

The choice of the artificial boundary $\hat{\Gamma}$ and the corresponding distribution of the source points usually depends on the smoothness of the geometry and on the regularity of the boundary conditions. The optimal choice of this parameters for the MFS still remains an open problem. From this point of view, an advantage of the PWM over the MFS is that no artificial boundary is necessary for its application. Another advantage of the PWM is that, for reasonable scale 2D problems, it is significantly faster than the MFS due to the faster evaluation of exponential functions (plane waves) than Hänkel functions (fundamental solutions).

Acknowledgments

The financial support received from the Fundação para a Ciência e a Tecnologia (FCT) Project UID/Multi/04621/2013 is gratefully acknowledged.

References

[1] Kupradze VD, Aleksidze MA. The method of fundamental equations for an approximate solution of certain boundary value problems. Comput Math Math Phys 1964;4:82–126.
[2] Mathon R, Johnston RL. The approximate solution of elliptic boundary-value problems by fundamental solutions. SIAM J Numer Anal 1977;14:638–50.
[3] Fairweather G, Karageorghis A. The method of fundamental solutions for elliptic boundary value problems. Adv Comput Math 1998;9:69–95.
[4] Fairweather G, Karageorghis A, Martin PA. The method of fundamental solutions for scattering and radiation problems. Eng Anal Bound Elem 2003;27:759–69.
[5] Trefftz E. Ein gegenstuck zum Ritzschen verfahren. In: Proceedings of 2er international kongress fur technical mechanik, Zurich; 1926. p. 131–7.
[6] Alves CJS. On the choice of source points in the method of fundamental solutions. Eng Anal Bound Elem 2009;33:1348–61.
[7] Bogomolny A. Fundamental solutions method for elliptic boundary value problems. SIAM J Numer Anal 1985;22:644–69.
[8] Katsurada M. Asymptotic error analysis of the charge simulation method in a Jordan region with an analytic boundary. J Fac Sci Univ Tokyo Sect 1A Math 1990;37:635–57.
[9] Barnett AH, Betcke T. Stability and convergence of the method of fundamental solutions for Helmholtz problems on analytic domains. J Comput Phys 2008;227:7003–26.
[10] Alves CJS, Valtchev SS. Numerical comparison of two meshfree methods for acoustic wave scattering. Eng Anal Bound Elem 2005;29:371–82.
[11] Valtchev SS. Asymptotic analysis of the method of fundamental solutions for acoustic wave propagation. In: Simos TE, Psihoyios G, Tsitouras C, editors. American institute of physics conference series. Volume 1281 of American institute of physics conference series; 2010. p. 1179–82.
[12] Antunes PRS. Numerical calculation of eigensolutions of 3D shapes using the method of fundamental solutions. Numer Methods Partial Differ Equ 2011;27(6):1525–50.
[13] Leblanc A, Lavie A. Solving acoustic nonlinear eigenvalue problems with a contour integral method. Eng Anal Bound Elem 2013a;37(1):162–6.
[14] Leblanc A, Lavie A. Iterative estimation of eigenmodes for acoustic cavities. Eng Anal Bound Elem 2013b;37(6):924–7.
[15] Karageorghis A, Lesnic D, Marin L. The PWM for the identification of a sound-soft interior acoustic scatterer. In: Marin L, Aliabadi MH, editors. Advances in boundary element and meshless techniques XVIII. EC; 2017. p. 19–26.
[16] Jin B, Marin L. The plane wave method for inverse problems associated with Helmholtz-type equations. Eng Anal Bound Elem 2008;32(3):223–40.
[17] Karageorghis A. The plane waves method for axisymmetric Helmholtz problems. Eng Anal Bound Elem 2016;69:46–56.
[18] Antunes P.R.S.. A numerical algorithm to reduce the ill conditioning in meshless methods for the Helmholtz equation. 2017 [submitted for publication].
[19] Huttunen T, Monk P, Collino F, Kaipio JP. The ultra-weak variational formulation for elastic wave problems. SIAM J Sci Comput 2004;25(5):1717–42.
[20] Zhang L, Tezaur R, Farhat C. The discontinuous enrichment method for elastic wave propagation in the medium-frequency regime. Int J Numer Methods Eng 2006;66(13):2086–114.
[21] Ladevze P, Arnaud L, Rouch P, Blanz C. The variational theory of complex rays for the calculation of medium-frequency vibrations. Eng Comput 2001;18(1/2):193–214.
[22] Moiola A. Plane wave approximation in linear elasticity. Appl Anal 2013;92(6):1299–307.
[23] Evans L.C.. Partial differential equations. Volume 19 of Graduate studies in mathematics, vol. 19. AMS. 1998.
[24] Hadamard J. Lectures on Cauchy problems in linear partial differential equations. London: Oxford University Press; 1923.
[25] Colton D, Kress R. Inverse acoustic and electromagnetic scattering theory. In: Volume 93 of Applied mathematical science. Berlin/Heidelberg: Springer-Verlag; 1998.
[26] Hansen P.C.. Rank-deficient and discrete ill-posed problems. SIAM. 1998.
[27] Kupradze V.D.. Potential methods in the theory of elasticity. Jerusalem: Israel Program for Scientific Translations. 1965.
[28] Kupradze V.D.. Three-dimensional problems of the mathematical theory of elasticity and thermoelasticity. Amsterdam: North-Holland; 1979.
[29] Alves CJ, Martins NF, Valtchev SS. Extending the method of fundamental solutions to non-homogeneous elastic wave problems. Appl Numer Math 2017;115:299–313.
[30] Lin J, Chen W, Sun L. Simulation of elastic wave propagation in layered materials by the method of fundamental solutions. Eng Anal Bound Elem 2015;57:88–95. RBF collocation methods.
[31] Antunes RS, Valtchev SS. A meshfree numerical method for acoustic wave propagation problems in planar domains with corners and cracks. J Comput Appl Math 2010;234:2646–62.